Comparing RotCFD Predictions of the Multirotor Test Bed with Experimental Results

Sarah Conley
Mechanical Engineer
NASA Ames Research Center
Moffett Field, CA, USA

Carl Russell
Aerospace Engineer
NASA Ames Research Center
Moffett Field, CA, USA

Kristen Kallstrom
Research Associate
Science and Technology Corporation
Moffett Field, CA, USA

Witold Koning
Aerospace Engineer
Science and Technology Corporation
Moffett Field, CA, USA

Ethan Romander
Aerospace Engineer
NASA Ames Research Center
Moffett Field, CA, USA

ABSTRACT

The Multirotor Test Bed (MTB) is a new capability for testing a wide array of advanced vertical take-off and landing (VTOL) rotor configurations, with a primary focus on testing in the U.S. Army 7- by 10-Foot Wind Tunnel at NASA Ames Research Center. The MTB was designed to allow adjustment of the vertical, lateral, and longitudinal placement of each rotor, as well as allow tilt adjustment of each rotor and pitch adjustment of the whole assembly. Each rotor can tilt forward 90 deg and backwards 5 deg. In addition, the entire MTB can tilt forward 20 deg and backwards 10 deg. This flexibility allows the system to be tested in many different configurations. There is a six-axis load cell under each rotor assembly, to measure both the steady and dynamic loads produced by each rotor. The wind tunnel scales can measure loads on the full assembly. The overall goal of the MTB project is to help gain a better understanding of the performance, control, interactional aerodynamics, and acoustics of multirotor systems. A hybrid CFD tool called RotCFD (Rotorcraft Computational Fluid Dynamics) was used to simulate the MTB in several testing configurations. This paper explains the method of running the RotCFD simulations and explores the results from the simulations. The objective of this paper is to compare the RotCFD simulation results with the MTB wind tunnel test data, seeking to further validate RotCFD for multirotor systems and assess the influence of aerodynamic interactions on individual rotor performance.

INTRODUCTION

Background

Advanced multirotor vertical flight aircraft concepts are emerging faster than rigorous individualized tests can investigate their utility and performance. Additionally, rotorcraft operate in a challenging environment of extremely complex aerodynamics that are difficult to accurately simulate with computational fluid dynamics (CFD) tools. Wind tunnel testing serves a critical role in providing validation data to help improve rotor performance predictions, but wind tunnel test data for multirotor systems have only recently started to become available.

Two previous NASA wind tunnel tests of multirotor UAS (Unmanned Aerial System) vehicles were conducted in October – December 2015 [Ref. 1] and January – February 2017 [Ref. 2 and 3], referred to as the MUAS1 and MUAS2 tests, respectively. The MUAS (Multicopter Unmanned Aerial System) tests measured the aerodynamic performance of five quadcopters (3DR SOLO, 3DR Iris+, DJI Phantom 3 Advanced, SUI Endurance, and the ARL Overlapped Quadrotor), a tilt-wing (Elytron 4S UAV), and an octocopter (Drone America x8). The MUAS1 test entry generated a high-quality set of performance data for these vehicles, but the test also raised additional questions, particularly related to vibrations, blade deflections, aerodynamic interference, acoustics, and trim strategies. The MUAS2 test expanded on the first test series by attempting to better characterize vibrations, interactional aerodynamics, and blade motion.

The MUAS tests had three main limitations:

- Loads were only measured for the entire vehicle, so a full picture of interactional aerodynamics could not be gleaned from the data.
- Testing was limited to existing vehicles with no ability to alter the configuration.
- Testing focused on small UAS, with blade chord-based Reynolds numbers below 100,000 – a regime with different rotor performance characteristics than those seen in typical Urban Air Mobility (UAM) and larger UAS applications.

The Multirotor Test Bed (MTB) program builds upon the knowledge and capabilities developed during the MUAS tests. By measuring individual rotor loads for a multirotor system and allowing for adjustments to rotor position and attitude, the MTB can provide a wealth of data on the aeromechanics of arbitrary multirotor configurations. The adjustment capabilities of the MTB allow the multirotor design space to be parametrically explored and optimized. The MTB is also at a larger scale than the small UAS that have been tested before, which allows for testing at Reynolds numbers more relevant to full-scale piloted electric vertical take-off and landing (eVTOL) aircraft. The assembled MTB in the U.S. Army 7- by 10-Foot Wind Tunnel is shown in Figure 1.

Presented at the Vertical Flight Society's 76th Annual Forum & Technology Display, Virginia Beach, VA, October 6-8, 2020.

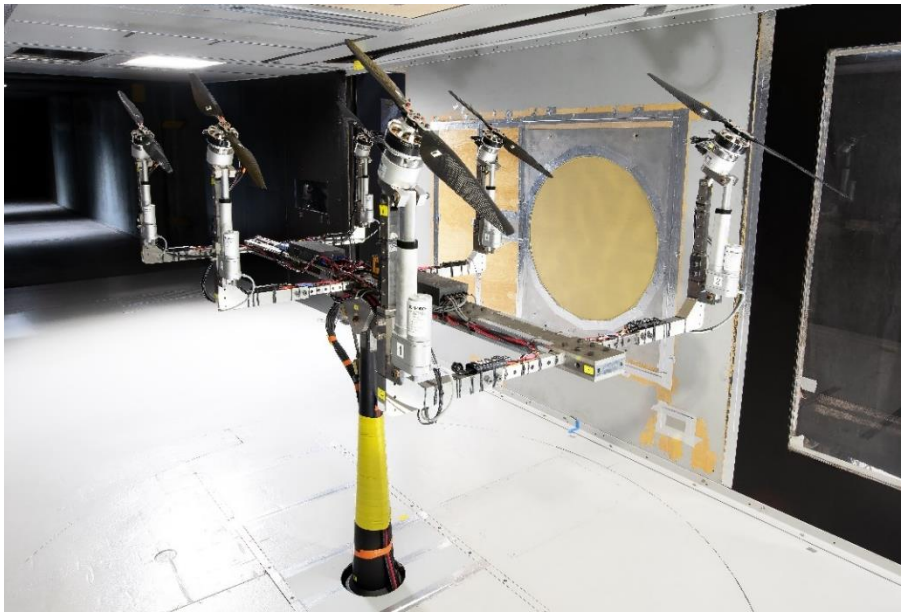

Figure 1: MTB in 7-by 10-Foot Wind Tunnel.

Many rotorcraft concepts with six (or more) rotors have been proposed by a number of different eVTOL companies, but significant testing is still required to evaluate key parameters including performance, safety, and comfort for human passengers. In addition to allowing for the evaluation of fundamental rotor-rotor interactions, the test capabilities of the MTB will be available for future tests of new multirotor aircraft concepts or rotor configurations. Such capability will aid in risk-reduction activities for organizations developing advanced eVTOL aircraft before committing to the expense and complexity of moving on to full-scale testing.

Design Overview

The Multirotor Test Bed consists of six individual rotor assemblies, each with its own lateral, vertical, longitudinal, and tilt adjustment systems. For the initial testing configuration, each fixed-pitch rotor has a 24.5 in diameter and the whole rotor assembly can tilt forward 90 deg and backwards 5 deg. The tilt system for each rotor uses a linear actuator that is controlled remotely during testing. Smaller rotors can be installed, but the ~2 ft diameter of the baseline configuration is the practical upper limit on rotor size for the MTB when installed in the 7- by 10-Foot Wind Tunnel. The central support of the test rig is the strongback, which acts as a structural backbone for the assembly. Lateral support beams are fixed to the strongback and connect to the adjusting L-brackets. The rotor assemblies are connected to the vertical support beams. The pitch adjustment for the strongback is controlled by a stepper motor interfacing with a jackscrew within the strut that supports the MTB in the wind tunnel. The strut is secured to the center of the wind tunnel turntable in the middle of the test section. The whole assembly can pitch 20 deg forward (nose down) and 10 deg backward (nose up). There are load cells under each rotor to capture loads and vibrations. A CAD model of the main upper assembly is shown in Figure 2.

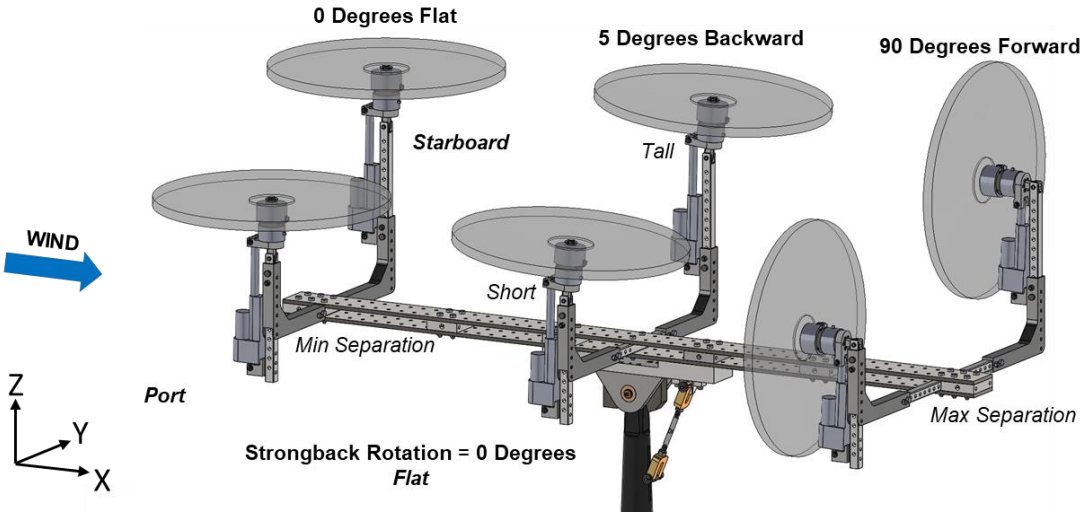

Figure 2: MTB, side view of assembly.

The total weight of the assembly is about 250 lb, not including the strut, which weighs approximately 340 lb. The maximum dimensions of the MTB are 80.63 in long by 63.2 in wide by 35.24 in tall (not including the strut). The MTB was tested in the U.S. Army 7- by 10-Foot Wind Tunnel at NASA Ames Research Center during the fall of 2019. The MTB was designed to withstand all planned testing conditions (with considerable margin) in the 7- by 10-Foot Wind Tunnel, as well as acquire accurate rotor force and moment measurements. An overview of the test and data is presented in Ref. 4. More details on the design of the MTB are provided in Ref. 5.

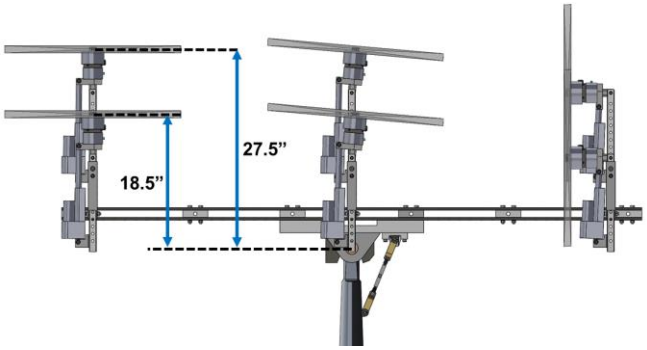

Figure 3: Side view of MTB with vertical dimensions of the rotors.

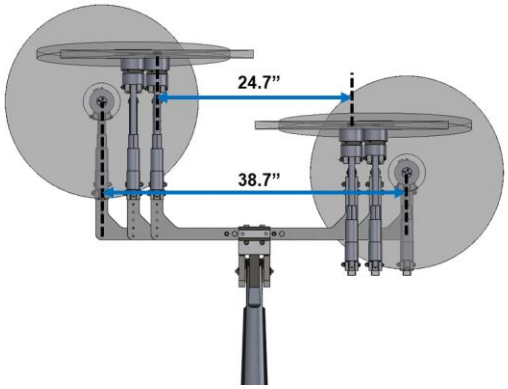

Figure 4: Front view of MTB with horizontal dimensions of the rotors.

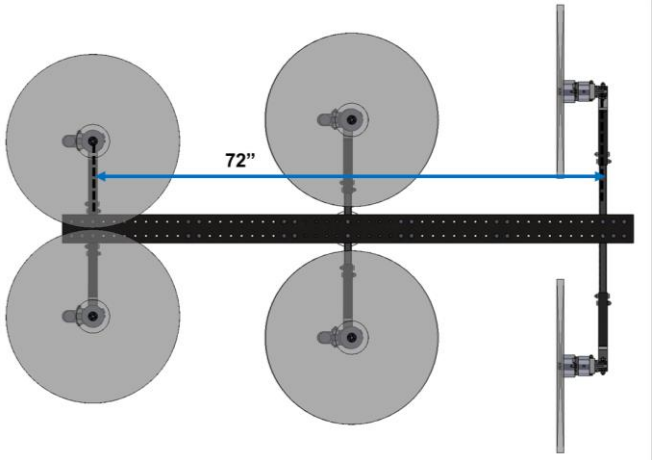

Figure 5: Top view of MTB with lengthwise dimension.

RotCFD

The design tool used for this analysis is a mid-fidelity computational fluid dynamics (CFD) program RotCFD (Rotorcraft CFD), developed by Sukra Helitek, Inc. RotCFD uses an Integrated Design Environment (IDE) specific to rotorcraft, bridging the worlds of design and CFD [Refs. 6 and 7]. The key components of RotCFD are a geometry module, a semi-automated grid generation module, a flow-solver module, a rotor module, and a flow visualization and analysis module, all integrated in one environment [Refs. 7 and 8]. These modules allow rotorcraft performance metrics and flowfields to be simulated over time and analyzed in a Graphical User Interface (GUI).

The rotor blades are modeled using a blade element method (BEM) and are represented through the momentum they impart on the flow. Normally in CFD applications, a fully viscous, unsteady, body-conforming grid is used to compute the flow induced by the rotor, but representing the rotors by momentum sources greatly reduces the computational time and complexity. The Reynolds-Averaged Navier-Stokes (RANS) equations provide the flowfield near the rotors using the rotor induced momentum sources and the blade element theory provides the forces on the rotor blades from the local velocity vector field. These equations are coupled implicitly to yield a self-contained method for generating unsteady performance, as well as the near and far wake including all the aerodynamic interferences present [Ref. 7]. The reduced complexity of the simulations allows for complex flowfields to be analyzed on a single workstation with good results [Ref. 9].

The rotor solution model used in RotCFD for this analysis is the actuator-disk model (ADM). A discrete-blade model is also available, but that model is more computationally expensive. The actuator-disk solution implicitly couples the external flowfield to the rotor via integrated momentum sources, whereas the discrete-blade solution couples the external flow to individual lifting lines, one for each blade [Ref. 10]. Both models require external airfoil tables so the program can calculate each blade section’s lift, drag, and pitching moment. These sectional forces and moments are then converted to source terms, which are added along the blade span (using BEM) or averaged over the azimuthal locations (using ADM).

This analysis uses the Rotorcraft Unstructured Solver (RotUNS) module which uses three-dimensional, unsteady Reynolds Averaged Navier-Stokes equations (URANS) on a Cartesian unstructured grid with tetrahedral body-fitting near the body [Ref. 9]. The Semi-Implicit Method for Pressure-Linked Equations Revised (SIMPLER) is a line of pressure based algorithms which are used with the under relaxation factors to iteratively compute the flowfield. Turbulence is accounted for by the URANS equations combined with a two-equation realizable k-ε turbulence model with special wall treatment [Ref. 9].

The internal grid generator, UGen, generates a Cartesian octree grid, starting from the boundary and then intersecting the body. The cells that intersect the geometry and the surrounding cells are sub-divided into tetrahedra, resulting in a grid that approximately conforms to the surface of the body.

RotCFD accepts inputs on the specific rotor geometry, rotor RPM, tunnel speed, and tunnel conditions, used in the MTB wind tunnel tests. RotCFD then outputs the flow solution and individual rotor performance. Because RotUNS is unsteady, the flow changes with time can be observed. This study is seeking to not only validate this tool, but also validate the methods by which this tool is implemented.

METHOD

Airfoil Tables

The MTB uses six KDE-CF245-DP two-bladed, 24.5 in carbon fiber rotors. The blades were 3D-scanned to generate an accurate three-dimensional geometry, which provides camber, thickness, chord, and twist characteristics. Twenty-five airfoil sections were identified along the span to provide accurate blade characteristics for use in simulations. Four primary airfoils were selected at radial stations of r/R = 0.1891, 0.2662, 0.7515, and 0.9435 based on their maximum thickness, thickness position, leading edge radius, maximum camber, and maximum camber positions. The characteristics of the four primary airfoils should accurately capture any spanwise variation in these parameters when using a limited number of airfoils for the rotor model.

Airfoil tables are created through two-dimensional (2D) computational analyses of an airfoil shape for a specified range of angle-of-attack and Mach number pairs or by wind tunnel testing. The 2D analysis computes the section lift coefficients, drag coefficients, and moment coefficients. The resulting tables of aerodynamic coefficients serve as input to more complex three-dimensional CFD analyses, as well as comprehensive analysis tools.

Although airfoil tables for the KDE rotor existed from previous research [Ref. 11], the sectional aerodynamic coefficients were calculated in that analysis using fully turbulent flow conditions. A subsequent simulation for the current study used XFOIL [Ref. 12] to show that for the expected operational conditions, transition of the boundary layer can occur under the present low-Reynolds number conditions. This evidence of boundary layer transition suggests that calculations from fully laminar or fully turbulent models could be prone to inaccuracies when used to calculate the lift, drag, and sectional moment coefficients as there is no control over the laminar-turbulent transition location without using a transition model. While accurate computation of laminar-turbulent transition using Reynolds-Averaged Navier-Stokes (RANS) based methods is non-trivial, XFOIL is capable of generating reasonably accurate aerodynamic coefficients quickly, with laminar-turbulent transition predictions following from linear stability theory.

The maximum and minimum Mach numbers were determined for a rotor operating at 2000 RPM in a freestream velocity of 40 ft/s – approximately the conditions experienced by the MTB rotors. Table 1 provides the calculated Reynolds numbers (Re) and the angle-of-attack range for each critical airfoil.

Table 1. Critical airfoil Re and α inputs for XFOIL.

		Re			
r/R	**α**	**M=0.01**	**M=0.1**	**M=0.2**	**M=0.3**
0.1891	-20° to 20°	7,365	73,645		
0.2662	-20° to 20°	11,032	110,322		
0.7515	-18.5° to 15°		89,466	178,932	
0.9435	-19° to 9°		54,848	109,695	164,543

The maximum Mach number refers to the maximum advancing local section Mach number of the airfoil, and the minimum Mach number refers to the retreating local section Mach number of the airfoil. These maximum and minimum Mach numbers provided the Mach number range needed for the airfoil tables. Because the MTB is operating within this range, the airfoil tables will ensure that the RotCFD rotor performance calculations are not based on extrapolated airfoil data.

For angles-of-attack exceeding the ranges specified in Table 1, XFOIL was unable to converge. The values highlighted in green in Table 1 are the Re values used for the airfoil tables, as they reflect the minimum and maximum Mach numbers experienced by the airfoil. For any cases that failed to converge, the sectional coefficient could be linearly interpolated if the failed case was between cases that achieved convergence.

The XFOIL output files containing the sectional lift, drag, and moment coefficients for each Mach number were blended with the NACA 0012 airfoil table using a MATLAB script and were properly formatted into a readable .c81 format using a .c81 file cleaner code. As a reminder, the NACA 0012 table was used for angles-of-attack outside of the range provided in Table 1, with limits at –180 and +180 deg. Calculating the transition location using the stability model in XFOIL results in a mid-chord transition from laminar to turbulent flow. That result is likely to be more accurate than assuming fully turbulent or fully laminar flow over the entire chord. This ensures that reasonable aerodynamic coefficients are used to simulate the entire operating range of the MTB rotors and avoids erroneous extrapolation that could impact rotor performance.

Test Matrix

All cases for the comparison study between the RotCFD simulation results and the MTB experimental data are given in the Appendix. These cases were chosen because only one independent variable changed for each case, and therefore the effects of each variable could be easily observed. The RPM for all cases was approximately 2000, and the diagram of the rotors and their positions relative to the MTB's orientation in the tunnel are shown in Figure 6. The six-axis load cells underneath each rotor provided the forces (Fx, Fy, and Fz) and moments (Mx, My, and Mz) measurements.

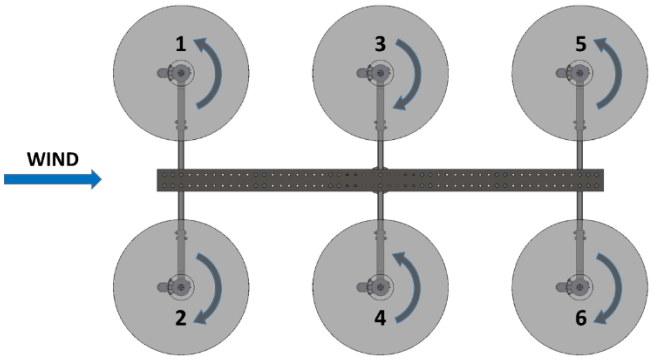

Figure 6: Top View of MTB with labeled rotor locations.

The coordinate system used for the tunnel is as follows: +x is going along the length of the tunnel in the same direction as the wind, +y is going towards the starboard, and +z is going up. Pitch refers to the pitching of the whole MTB. Although the rotors can also individually tilt forward 90 deg and backwards 5 deg (independent of the strongback), only runs where the rotors are not tilted (at 0 deg) are used in this comparison study. Therefore, for all cases in this study, the rotor plane remains parallel to the strongback. So, when the MTB pitches -10 deg, the rotors are also pitched -10 deg relative to the tunnel coordinate system. Additionally, negative pitch is defined as nose down and positive as nose up.

Most of the runs examined in this paper are with the MTB rotors in their minimum-height configuration (referred to as the short rotor configuration), that is 2.3 diameters (D) above the tunnel floor at zero shaft angle and zero model pitch (Figure 10). A few of the six-rotor cases (cases 12.1 – 12.12) were 2.6D above the tunnel floor at zero model pitch, or 7 in higher than the short rotor configuration (referred to as the tall rotor configuration). The pitch angle of the MTB is varied for the different cases between -10 and 0 deg. The wind tunnel speed, static pressure, static temperature, static density, dynamic viscosity in the wind tunnel, and individual rotor RPM were recorded/calculated for each data point. These values were then used in the RotCFD simulations of the different cases. The pitch angle of the MTB was assumed to be exactly -10, -5, or 0 deg for the different cases. The exact tunnel conditions for each case as obtained during testing were used in the CFD simulations to eliminate any potential additional source of inaccuracy.

There are three different types of cases that were used in this RotCFD comparison study:

- TwithB – "Tunnel with Body" – The simulation has the rotors and body of the MTB in a simulated tunnel (boundary of the simulation is the dimension of the tunnel walls), see Figures 8, 9, and 10.
- FF – "Free Field" – The simulation significantly extends the computational boundary to reduce the effects that the boundary would have on the flow. Essentially, the FF cases are rotors floating in mid-air with no body. The minimum clearances that each rotor has from its center to each boundary wall are: 6.5D in front (x-axis), 12D in the back (x-axis), 9.6D to the sides (y-axis), 6D above (z-axis), and 10.7D below (z-axis), see Figure 7. The simulation excludes the body of the MTB.
- TnoB – "Tunnel no Body" – The simulation is in a simulated tunnel without the body of the MTB. Comparing results between the TwithB and the TnoB cases highlights the effects of the body on the flow and rotor performance. Comparing the results of the FF and the TnoB cases highlights the effects of the tunnel on the flow and rotor performance.

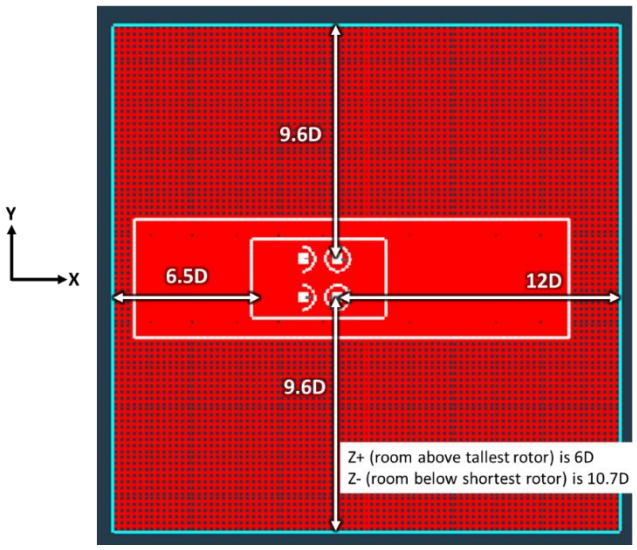

Figure 7: Free Field Grid, top view (wind flowing from left to right).

The full test matrix is given in the Appendix. Table 2 below is a summary of the different cases that were examined in this study. The number of rotors in the different cases are either 1, 2, 4, or 6, with tunnel speeds of 20 and/or 40 ft/s, and the rotors are in the tall or short rotor configuration. Note that only the single rotor configurations have TwithB, FF, and TnoB cases. All the other rotor configurations only have TwithB and FF cases.

Table 2: Summary of MTB RotCFD Test Matrix

Number of Rotors	Tunnel Speed [ft/s]	MTB Rotor Config.	MTB Pitch [deg]	Case Types	Case Numbers
1	20, 40	Short	-10, -5, 0	TwithB, FF, TnoB	11.1-11.18
2	20	Short	-10, -5, 0	TwithB, FF	16.1-16.6
4	20	Short	-10, -5, 0	TwithB, FF	15.1-15.6
6	20, 40	Tall, Short	-10, -5, 0	TwithB, FF	12.1-12.12 and 13.1-13.12

Gridding

The objective was to find a balance between the accuracy of the results, computational budget, and time availability. Care was taken to ensure that the grid around the body of the MTB and the rotors remained the same throughout all cases. This was done to reduce the potential of additional inaccuracies and to increase the confidence in the comparisons between cases.

For the TwithB cases, the grid at the boundary (which acted as the tunnel walls) was also refined to provide a minimum required grid for the boundary layer on the wall to develop. Several refinement boxes, which are boxes in which the grid can locally be refined, were used in generating the grids. A refinement box was created around the body of the MTB, and additional refinement boxes were generated around the rotors, as shown in Figures 9 and 10. These refinement boxes, both around the body, and around the rotors, remained the same for all cases. A rotor refinement box was included only if a rotor was present (e.g. for the single rotor cases, there was only one rotor refinement box around rotor 2). The number of cells within the refinement boxes changed depending on the angle of the MTB because the rotor refinement box faces remain parallel to the inertial Cartesian coordinate system. For example, when the MTB was pitched forward 10 deg, the rotor refinement boxes increased in size, in order to contain the whole rotor (Figure 9). Although the cell count increased, the cell size did not change since the refinement level remained constant. Additionally, body fitting was implemented in the grid to more accurately model the MTB in the simulation. Note that in Figures 8, 9 and 10, the flow direction is in the positive X direction, going from left to right.

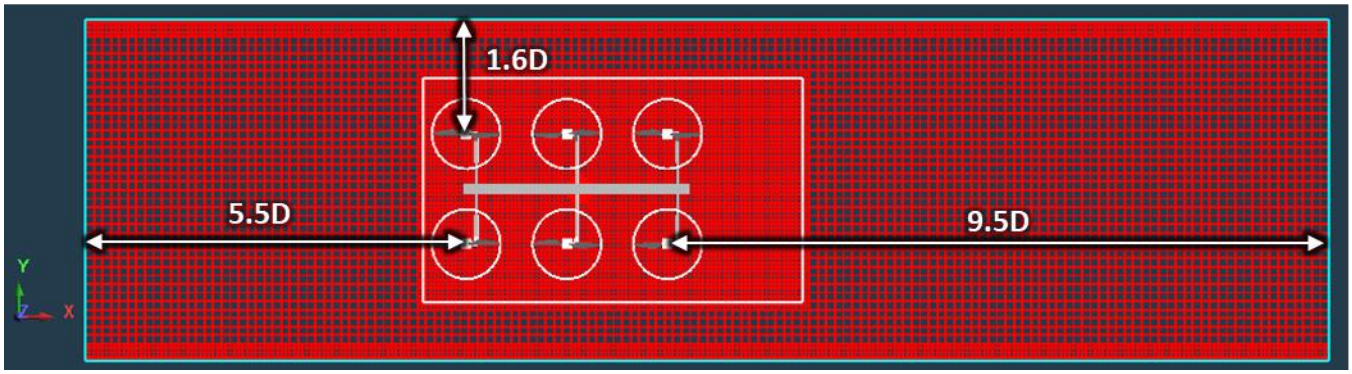

Figure 8: Top view of TwithB grid. Case 12.1 and 12.4 – Tall Rotor configuration, pitched -10 deg.

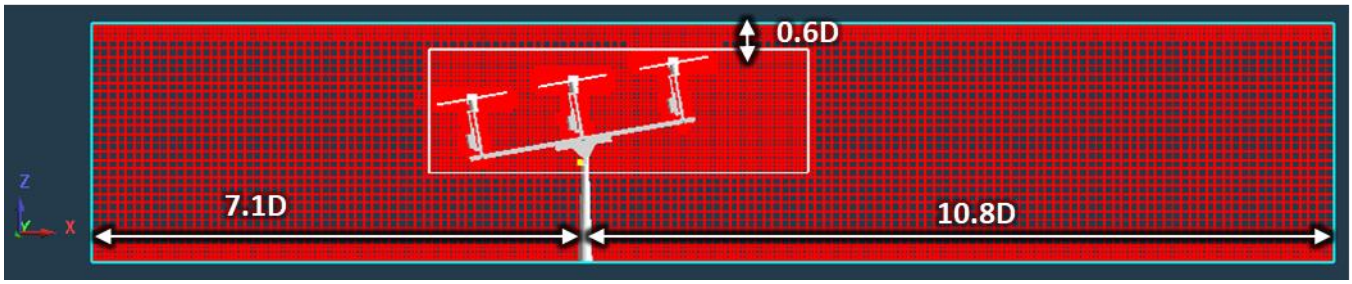

Figure 9: Side view of TwithB grid. Case 12.1 and 12.4 – Tall Rotor configuration, pitched -10 deg.

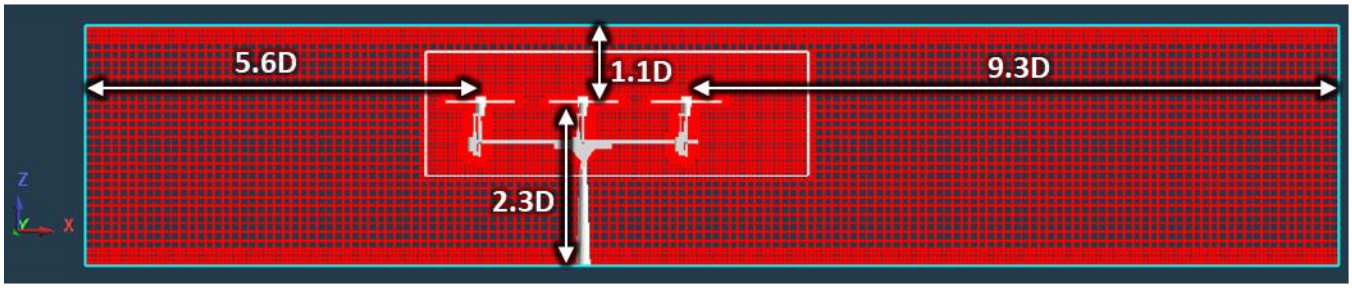

Figure 10: Side view of TwithB grid. Case 12.3 and 12.6 – Short rotor configuration, 0 deg pitch.

For the TnoB cases, the grid parameters were essentially the same as the TwithB cases, except the cell count decreased since there was no body and the grid did not need to adapt and refine to the MTB geometry (no body fitting).

For the FF cases, the boundary was extended past the tunnel walls, as seen in Figure 7. For these cases, two refinement boxes were used in conjunction with the rotor refinement boxes. These refinement boxes were given the names “tunnel refinement box” and “model refinement box”.

The tunnel refinement box has the same dimensions and cell size as the tunnel (the same as the boundary in the TwithB cases). The model refinement box has the same dimensions and cell size as the refinement box around the model in the TwithB cases. The idea behind these refinement boxes was to keep the grid as similar as possible to the TwithB cases in order to compare between the cases more accurately. The refinement levels and number of cells were calculated to ensure that the size of the cells within the tunnel refinement box and the model refinement box matched exactly with the TwithB case grids. The cell sizes for the FF cases outside of the tunnel refinement box were made larger in order to keep the total cell count manageable. Additionally, the boundary walls for the FF cases were not refined and were all set to the tunnel velocity except for X-Max (where the flow exits the simulation), which remained set to Mass Outflow Correction.

Simulation Parameters

The physical simulation time was set to the time required for the freestream velocity to traverse the domain (in the x-direction) twice. The boundary was made larger than the actual wind tunnel test section (which is only 15ft long) in order to ensure that the flow had enough time and space to properly develop. In Ref. 13, Moffett set the test section length to be 26 ft. In the present study the test section length was extended to 36.5 ft (11.1252 m). Moffett also used on average 10,000 timesteps for most of the cases. For the present study, 20,000 timesteps were sufficient for most cases, and for a few of the less intensive cases, 15,000 timesteps proved to be sufficient in converging the rotor performance.

Running Cases

The cases were run on the Pleiades supercomputer at NASA Ames Research Center. RotCFD can be run on standard workstations, but was run on Pleiades in order to complete several cases in a short time period. Each case was run on a single Sandybridge+GPU node of the Pleiades computer. Using the node's NVIDIA Tesla K40 accelerator, RotUNS achieved performance on the order of 10-45 wallclock seconds per timestep (about four days total per case on average). Since many of these nodes were available on the Pleiades computer, the cases were run in parallel and all cases were completed in approximately two weeks. The simulation results and measured data were analyzed using Python scripts with the numpy and matplotlib libraries.

RESULTS AND ANALYSIS

In this section, the RotCFD results are presented and compared to the equivalent runs in the experimental data. Ref. 4 presents the experimental data capabilities of the MTB with the aim of explaining some of the phenomena and trends that can be observed from the different testing configurations. This paper aims only to compare the RotCFD results with the experimental data.

Isolated Rotor in Hover

A simple isolated rotor study was performed to verify that the RotCFD rotor model and simulation were set up correctly. For this study, the RPM of rotor 2 was varied between 500 and 6,000 RPM in hover without the presence of the MTB or wind tunnel walls. Due to time limitations, in the first round of MTB testing, only one data point for a single rotor in hover was taken. This data point was plotted against the values from the predicted isolated rotor cases and correlation between the points was very promising (see Figures 11 – 13). The rotor manufacturer data can be found at https://www.kdedirect.com/collections/uas-multi-rotor-brushless-motors/products/kde7215xf-135. Future MTB testing will include isolated rotor testing so that the rotor model can be further validated in hover.

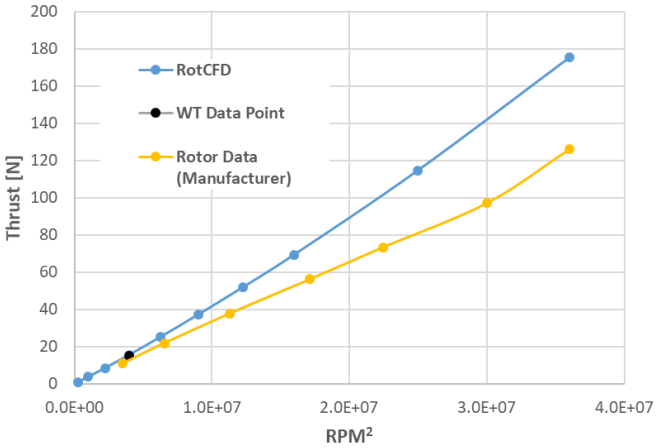

Figure 11: Isolated Rotor – Thrust vs. RPM².

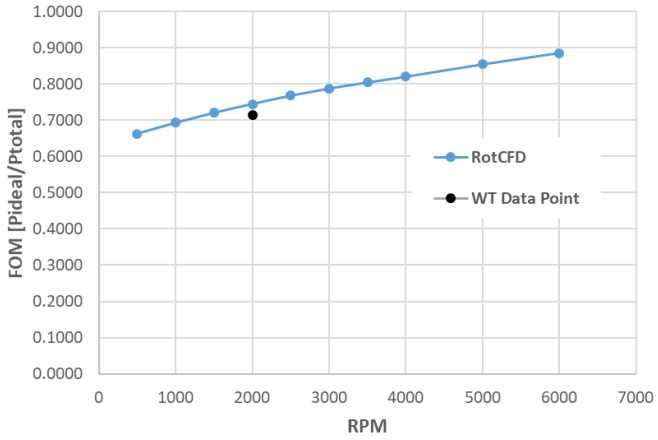

Figure 12: Isolated Rotor – FOM vs. RPM.

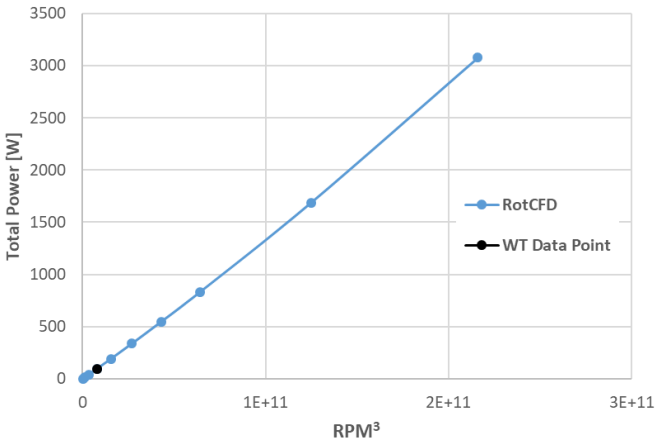

Figure 13: Isolated Rotor – Power vs. RPM³.

Single Rotor

The single rotor cases were run with Rotor 2, cases 11.1 – 11.18. The maximum discrepancies between the TwithB cases (11.1 – 11.6) and the experimental data for thrust and torque are 5.6% and 7.5% respectively. The average discrepancies for the TwithB cases for thrust and torque are 2.7% and 4.4% respectively. The equation used to calculate the discrepancy was:

$$Discrepancy = 1 - \frac{RotCFD}{Experimental} * 100\%$$

The average discrepancy is the average of the absolute values of the discrepancies. The cases with the best correlation were those with a 0 deg pitch angle (cases 11.3 and 11.6). The RotCFD values for the thrust are closer to the experimental values for a 0 deg pitch angle and at higher speeds (Figure 14). Torque has better correlation for zero pitch angle but no trend is observed for higher or lower tunnel speeds (Figure 15). Additionally, for these cases, RotCFD slightly under-predicts the thrust and over-predicts the torque values. The RotCFD results capture the trends in the experimental data for changes in tunnel speed (i.e. the deltas between the RotCFD values for 20 ft/s and 40 ft/s match those of the experimental values). All RotCFD simulation results were averaged over the last three rotor rotations.

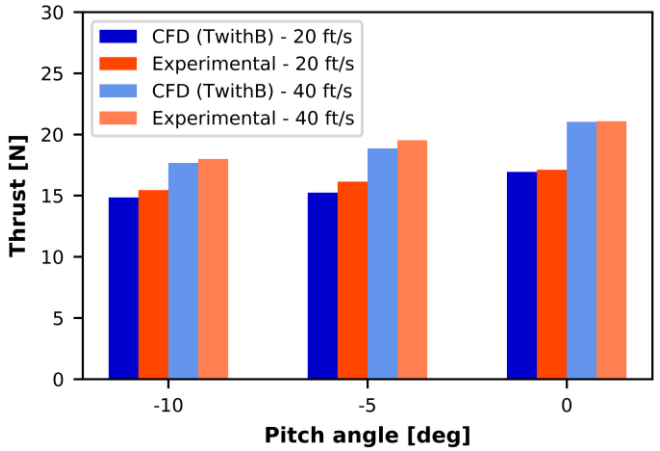

Figure 14: Single Rotor – TwithB vs Experimental – Thrust.

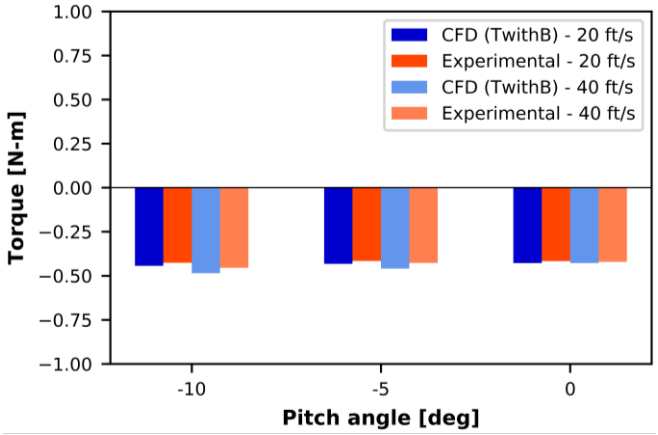

Figure 15: Single Rotor – TwithB vs Experimental – Torque.

For rotor performance coefficients, the thrust and torque coefficients show good correlation, but other force and moment coefficients are further off. These results could be due to any of the following reasons:

- The values for the other coefficients are very small.
- RotCFD does not accurately model some characteristics of the flow.
- The load cells were only able to accurately measure torque and thrust

Figure 16 shows the comparison between the RotCFD results for the TwithB case 11.1 with the corresponding experimental data.

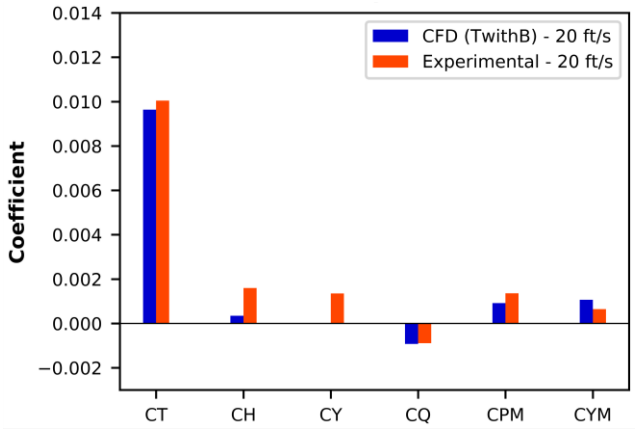

Figure 16: Single Rotor – TwithB vs Experimental – Coefficients, 20 ft/s, -10 deg pitch.

The experimental coefficients were calculated using the following formulas:

$$C_T = \frac{T}{\rho A(\Omega R)^2} = \text{Thrust Coefficient}$$

$$C_H = \frac{H}{\rho A(\Omega R)^2} = \text{H-Force Coefficient}$$

$$C_Y = \frac{Y}{\rho A(\Omega R)^2} = \text{Side Force Coefficient}$$

$$C_Q = \frac{Q}{\rho A(\Omega R)^2 R} = \text{Torque Coefficient}$$

$$C_{PM} = \frac{M_y}{\rho A(\Omega R)^2 R} = \text{Pitching Moment Coefficient}$$

$$C_{YM} = \frac{M_x}{\rho A(\Omega R)^2 R} = \text{Rolling Moment Coefficient}$$

[Ref. 14]

where ρ is density, A is rotor area, Ω is rotor speed in radians/sec, R is radius, T is thrust, H is H-force, Y is side force, and Q is torque. The RotCFD values for torque, torque coefficient, and rolling moment coefficient, were multiplied by -1 to match the coordinate system of the experimental data. The drag coefficient CH aligns with the x-axis of the tunnel coordinate system, and the side force coefficient aligns with the y-axis of the tunnel coordinate system.

The effect of the MTB body and the wind tunnel walls is discussed next. The TwithB cases exhibited the best correlation with the experimental data followed closely by TnoB, while the results from the FF differed the most from the experimental results. The TnoB and FF results imply that the body does have a large effect on the RotCFD simulations, but the effect from the tunnel is significantly greater. Since the TnoB cases were fairly similar to the TwithB cases, studies with more than one rotor prioritized the TwithB cases and the FF cases. The discrepancies in thrust between the FF simulations and the experimental data were greatest at 0 deg pitch angle for both tunnel speeds. The thrust actually decreased going from -5 deg pitch angle to 0 deg pitch angle for the FF cases, but it increased for the TwithB cases, TnoB cases, and the experimental data. At 0 deg pitch angle, rotor 2 is closer to the tunnel ceiling and therefore both the measured thrust and the thrust computed with tunnel walls (TwithB and TnoB cases) is increased. Thus, for the single rotor case, the effect of the tunnel on thrust is much more prominent for lower pitch angles. See Figures 17 – 20.

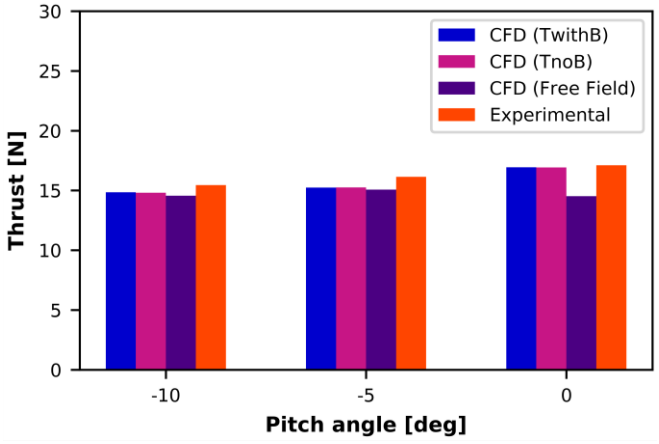

Figure 17: Single Rotor – 20 ft/s – Thrust.

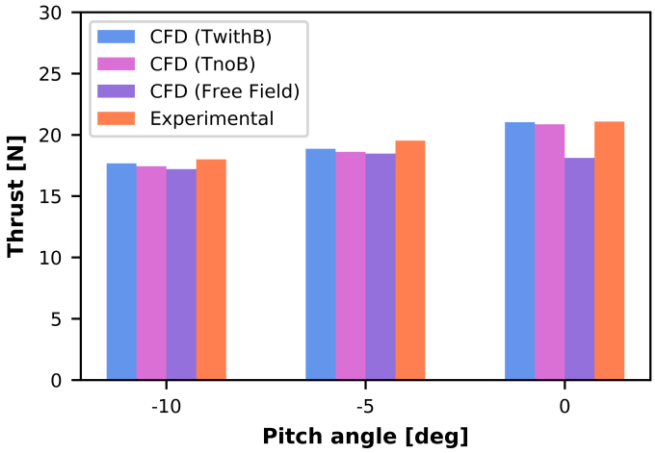

Figure 18: Single Rotor – 40 ft/s – Thrust.

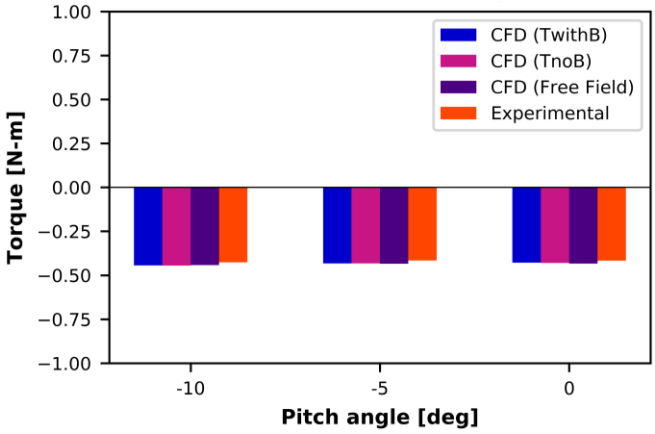

Figure 19: Single Rotor – 20 ft/s – Torque.

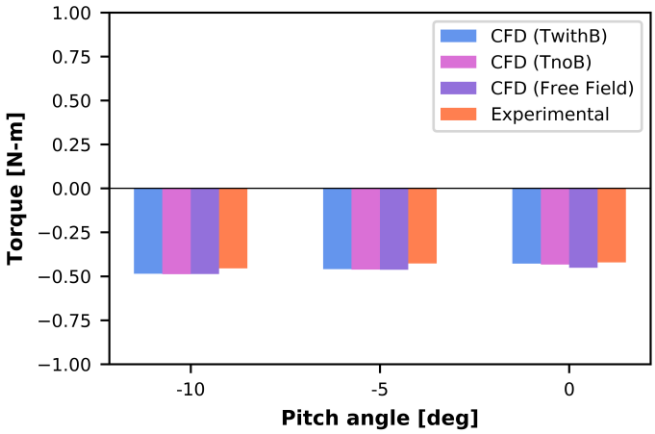

Figure 20: Single Rotor – 40 ft/s – Torque.

Two Rotors

For the two-rotor study cases 16.1 – 16.6, rotors 3 and 4 were simulated for -10, -5, and 0 deg MTB pitch angle, at 20 ft/s tunnel speed, in the short rotor configuration. The computed thrust for rotor 4 differed from experimental measurement by an average of 3.8% while computed thrust for rotor 3 differed by an average of 3.1% (i.e. percentages are the averaged discrepancies for cases 16.1 – 16.3), Figure 21. However, the computed torque (Figure 22) for rotor 4 differed from experimental measurement by an average of 11% while

computed torque for rotor 3 differed by an average of 3.3%. If both rotors have identical geometries and were located symmetrically in the test section, then the measured thrust and torque of rotors 3 and 4 should be equal (like the simulated results). Possible reasons for the differences in measured thrust and torque are: the load cell calibration issues or the influence of vibrations/resonances affecting the load cells unequally. The difference in measured thrust between rotors 3 and 4 is -0.375 N for -10 deg pitch angle, -1.02 N for -5 deg pitch angle, and -1.02 N for 0 deg pitch angle (thrust for rotor 3 was consistently lower than thrust for rotor 4). Rotors 3 and 4 are noted as R3 and R4 respectively in Figures 21 – 25.

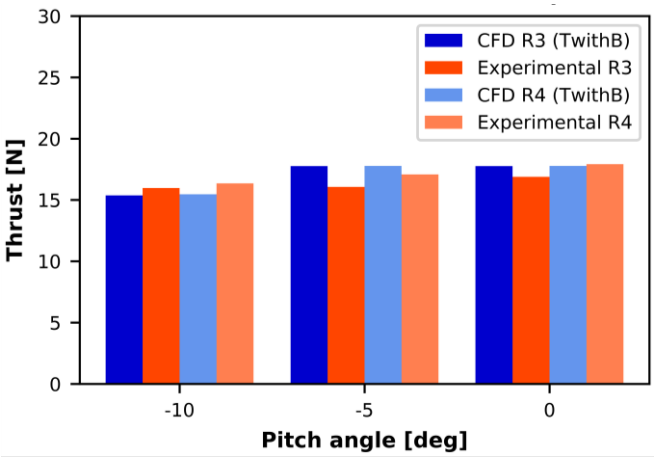

Figure 21: Two-Rotors – TwithB vs Experimental – Thrust.

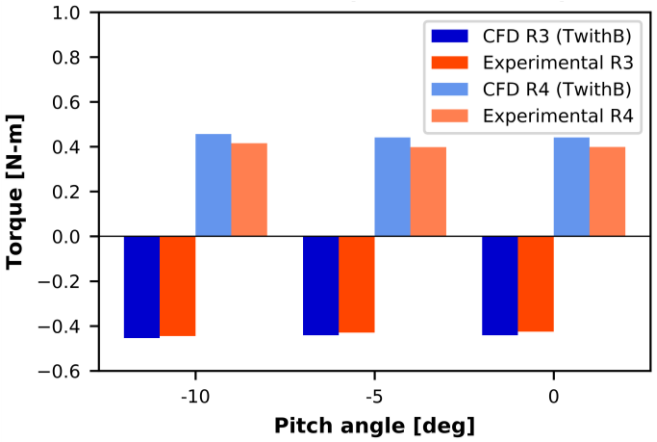

Figure 22: Two-Rotors – TwithB vs Experimental – Torque.

Similar to the single rotor case, the thrust and torque coefficients show good correlation with the experimental values, but the other coefficients do not (Figure 23).

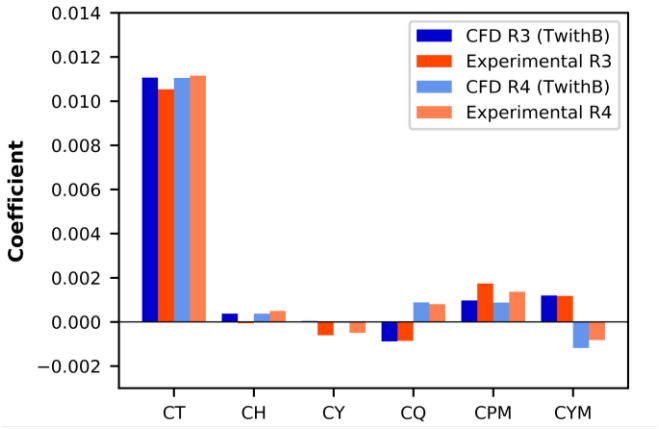

Figure 23: Two-Rotors – TwithB vs Experimental – Coefficients at 0 deg Pitch angle.

For the TwithB cases, the maximum discrepancy values for thrust and torque were 5.4% and -12.4%, respectively (Figures 24 and 25). The average discrepancies for the TwithB cases for thrust and torque were 3.5% and 7.1%, respectively. For the FF cases, at a pitch angle of 0 deg, the discrepancy for the thrust value is 15%. This further suggests that the tunnel and the body have a large effect on the flow at a pitch angle of 0 deg. From the previous section, it was shown that the tunnel had a much larger effect on the rotor performance than the body.

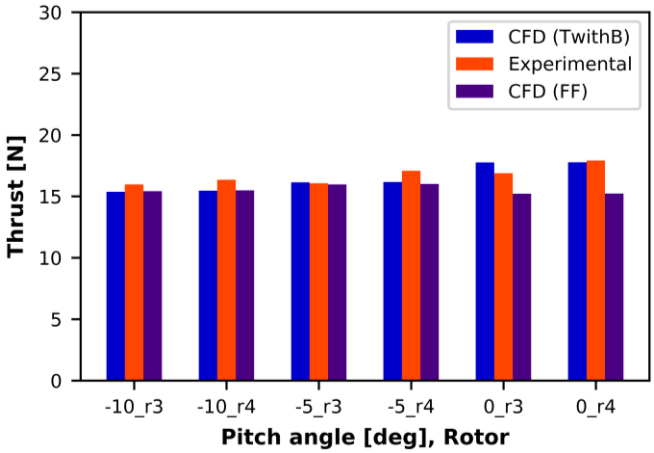

Figure 24: Two-Rotors – TwithB vs Experimental vs FF – Thrust for all Pitch angles.

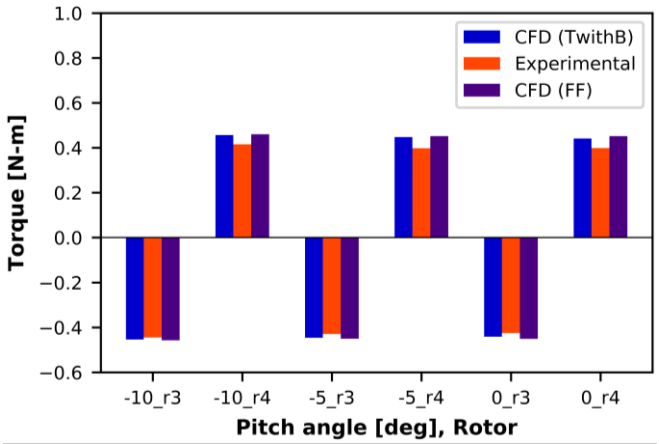

Figure 25: Two-Rotors – TwithB vs Experimental vs FF – Torque for all Pitch angles.

Four Rotors

For this study, rotors 1, 2, 3, and 4, (noted as R1, R2, R3, and R4 in the following figures) were simulated for the conditions defined in cases 15.1 – 15.6. For thrust and torque, rotors 1 and 4 were the most different from the experimental values. Figures 26 and 27 compare the rotor performance coefficients from the RotCFD TwithB case 15.1 (pitch angle -10 deg and 20 ft/s) with the experimental data. Figure 26 shows the values for rotors 1 and 2 and Figure 27 shows the values for rotors 3 and 4. For all TwithB cases, the maximum discrepancies for thrust and torque were 13.3% and 16.6% respectively. For the TwithB cases, the average discrepancies for thrust and torque were 8.2% and 7.5%, respectively (percentages averaged for cases 15.1 – 15.3 for all rotors).

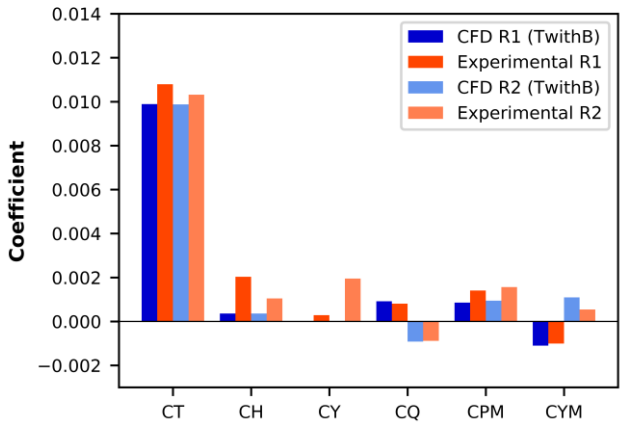

Figure 26: Four-Rotors – TwithB vs Experimental – Rotors 1 and 2 – Coefficients for Pitch angle -10 deg and tunnel speed 20 ft/s.

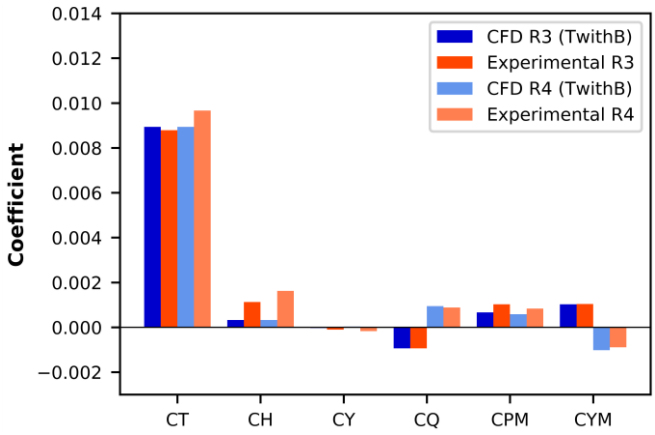

Figure 27: Four-Rotors – TwithB vs Experimental – Rotors 3 and 4 – Coefficients for Pitch angle -10 deg and tunnel speed 20 ft/s.

Comparing these results to the previous results shown for fewer rotors, the discrepancies between the RotCFD TwithB cases and the experimental data does seem to increase with increasing the number of rotors. Figure 28 compares the TwithB, Experimental, and FF results at a pitch angle of -10 deg, and Figure 29 compares the cases at a 0 deg pitch angle. Like the other studies, the discrepancies for the FF cases are larger than the TwithB cases, and increase with decreasing pitch angle, further supporting the theory that the tunnel and body effects the rotor performance the most at lower pitch angles, where the front rotors are closest to the ceiling. Based on symmetry, rotors 1 and 2 should have very similar performance. Rotors 3 and 4 are expected to suffer from degraded performance, compared to rotors 1 and 2, as they are operating in the wakes of rotors 1 and 2. Both the measurements and the simulations confirm this expected result.

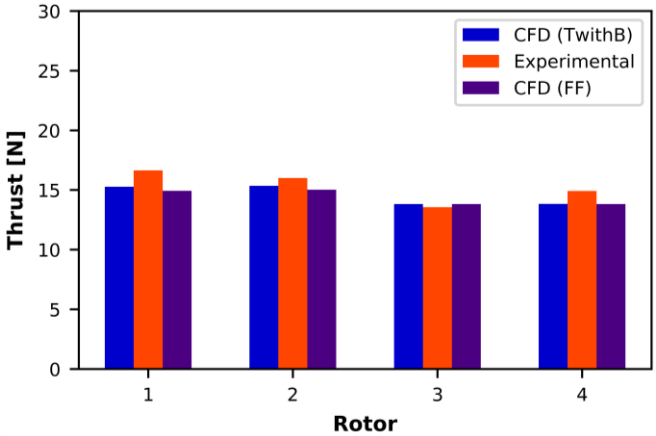

Figure 28: Four-Rotors – TwithB vs Experimental vs FF – Thrust for Pitch angle -10 deg and tunnel speed 20 ft/s.

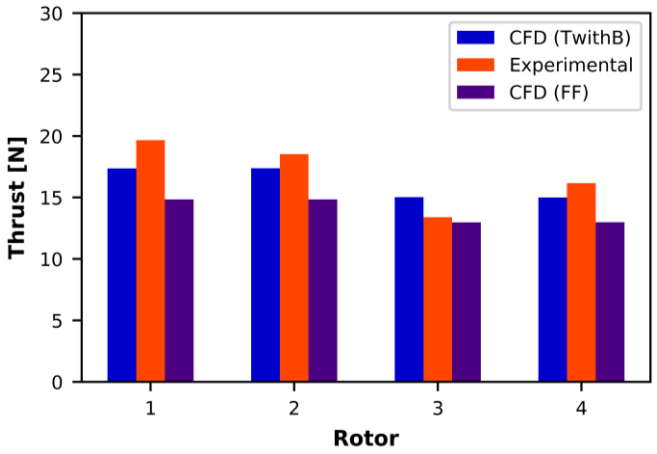

Figure 29: Four-Rotors – TwithB vs Experimental vs FF – Thrust for Pitch angle 0 deg and tunnel speed 20 ft/s.

Six Rotors

For the six-rotor cases, two simulation studies were performed: 1) cases 12.1 – 12.12, rotors in the MTB's tall rotor configuration, and 2) cases 13.1 – 13.12, rotors in the MTB's short rotor configuration. These cases were simulated for wind tunnel speeds of 20 ft/s and 40 ft/s. Since all previous studies were done in the short rotor configurations, cases 13.1 – 13.12 will be presented first.

Cases 13.1 – 13.6 were TwithB cases, with 13.1 – 13.3 being at 20 ft/s and 13.4 – 13.6 being at 40 ft/s tunnel wind speed. Figures 30 and 31 show the percent difference between the TwithB simulation results and the experimental data values for thrust. For cases 13.1 – 13.6, the results are presented in Figures 30 – 33 in the form of discrepancies in order to easily visually compare between the different cases. A positive discrepancy indicates under-prediction by RotCFD and a negative discrepancy indicates over-prediction by RotCFD.

Figures 30 and 31 show that the discrepancies for thrust are much larger for a pitch angle of 0 deg than for a pitch angle of -10 deg. This suggests that the RotCFD simulation may not be fully capturing the effects of interference. At 0 deg pitch, more rotor-rotor interference is expected than for the negative pitch cases. Additionally, the discrepancies for the thrust values are higher for the back four rotors (3, 4, 5, and 6) than for the front two rotors. These values also increase when the wind tunnel speed is increased from 20 ft/s to 40 ft/s. Figures 32 and 33 show the discrepancies for the torque values at 20 ft/s and 40 ft/s respectively. The discrepancies for the torque values are overall slightly higher for a pitch angle of 0 deg than for -10 deg, but the difference is much greater and more visible for thrust.

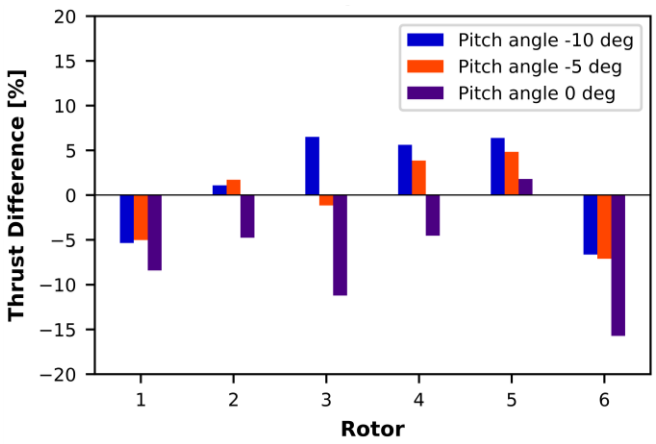

Figure 30: 6-Rotors (Short) – Discrepancies for 20ft/s TwithB Cases – Thrust.

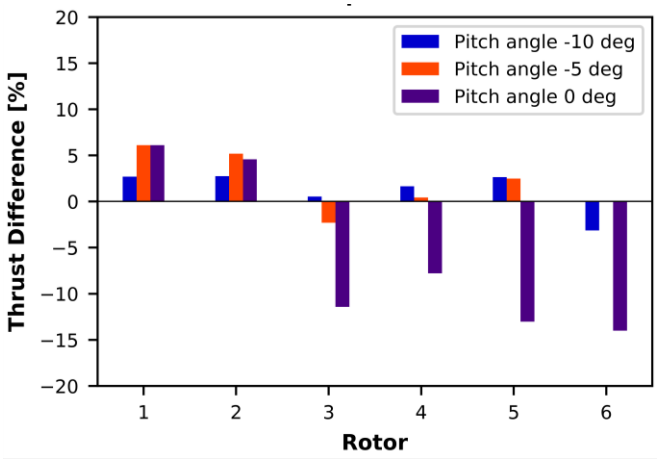

Figure 31: 6-Rotors (Short) – Discrepancies for 40ft/s TwithB Cases – Thrust.

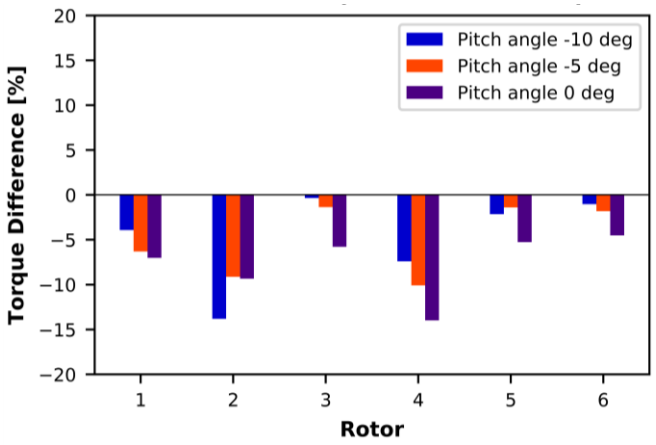

Figure 32: 6-Rotors (Short) – Discrepancies for 20ft/s TwithB Cases – Torque.

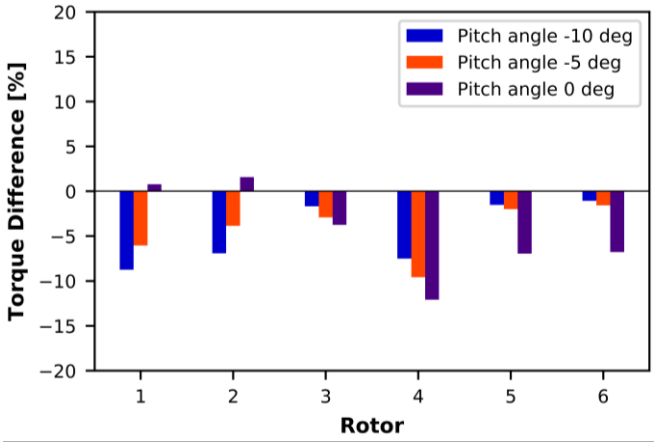

Figure 33: 6-Rotors (Short) – Discrepancies for 40ft/s TwithB Cases – Torque.

Figures 34 and 35 show the thrust values for all rotors in the short rotor configuration for the 20 ft/s and 40 ft/s cases respectively, in order to compare between the RotCFD results and the experimental data for the different rotors at different pitch angles. Both the RotCFD results and the experimental data show similar trends, i.e. both decrease in thrust as pitch angle goes from 0 deg to -10 deg, the thrust in the front rotors are higher than those of the back rotors, and the thrust delta is greatest for 0 deg pitch and smallest for -10 deg pitch.

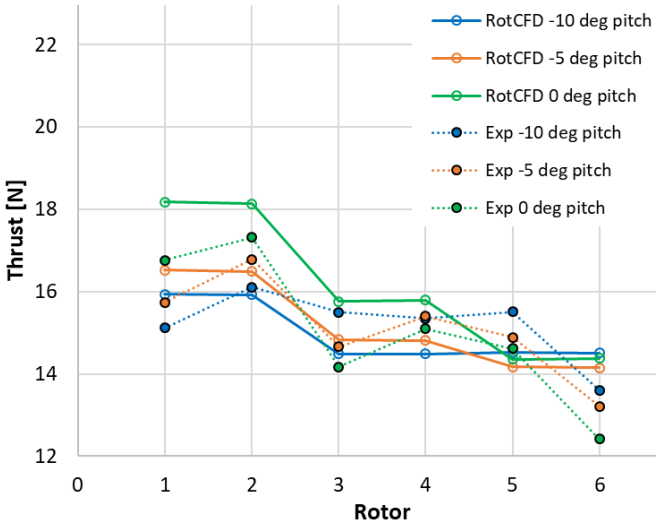

Figure 34: 6-Rotors (Short) – TwithB vs Experimental Thrust Values for 20 ft/s.

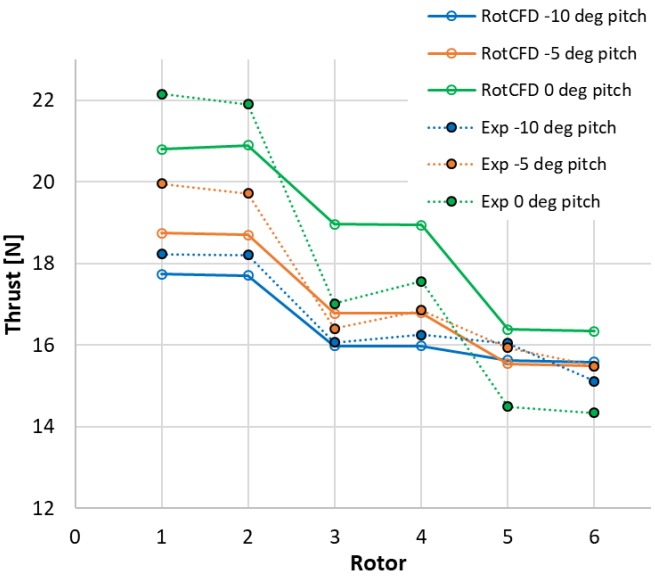

Figure 35: 6-Rotors (Short) – TwithB vs Experimental Thrust Values for 40 ft/s.

For Cases 13.1 – 13.6 the largest discrepancies for thrust and torque were -15.7% and -14%, respectively. The average discrepancy values for the TwithB cases for thrust and torque were 5.2% and 5.3%, respectively. The average discrepancy values for the six-rotor cases are less than those for the four-rotor cases (compare to 8.2% and 7.5% for thrust and torque respectively). It was predicted that increasing the number of rotors would increase the discrepancies between the RotCFD results and the experimental data, but the discrepancies did not increase going from four rotors to six rotors.

Cases 13.7 – 13.12 were FF cases. The discrepancies for the FF cases are only slightly higher than the TwithB cases. One interesting note is that for the higher tunnel wind speed of 40 ft/s the thrust discrepancies between the FF RotCFD results and the experimental data (Figure 36) are higher for the front rotors and the discrepancies between the TwithB RotCFD results and the experimental data (Figure 31) are higher for the back rotors. This trend is particularly visible for 0 deg pitch angle cases. The thrust is under-predicted for rotors 1 – 5 for all pitch angles.

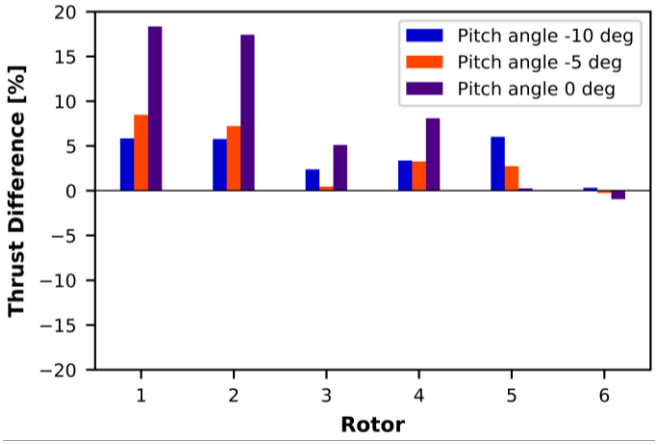

Figure 36: 6-Rotors (Short) – Discrepancies for 40ft/s FF Cases – Thrust.

Next are the six-rotor cases in the tall rotor configuration: cases 12.1 – 12.6 are TwithB and cases 12.7 – 12.12 are FF. Similar to the short rotor configuration cases (13.1 – 13.12), the first three cases of each set (12.1 – 12.3 and 12.7 – 12.9) are for a tunnel speed of 20 ft/s and the next three cases (12.4 – 12.6 and 12.10 – 12.12) are for a tunnel speeds of 40 ft/s with varying pitch angles. The full test matrix is provided in the Appendix.

Looking at the TwithB cases first, the trends seen for the tall rotor configurations are different than the short rotor configuration cases. For starters, the thrust discrepancies for the 20 ft/s cases are relatively similar for all pitch angles, with the exception of the front two rotors having slightly higher discrepancies for a pitch angle of 0 deg (Figure 37). For the higher wind tunnel speed of 40 ft/s, the discrepancies are fairly low for both pitch angle of -10 and -5 deg. For the pitch angle of 0 deg, however, the front two (rotors 1 and 2) and back two rotors (rotors 5 and 6) show high discrepancies with the thrust of the front two rotors under-predicting, and the back two rotors over-predicting (Figure 38).

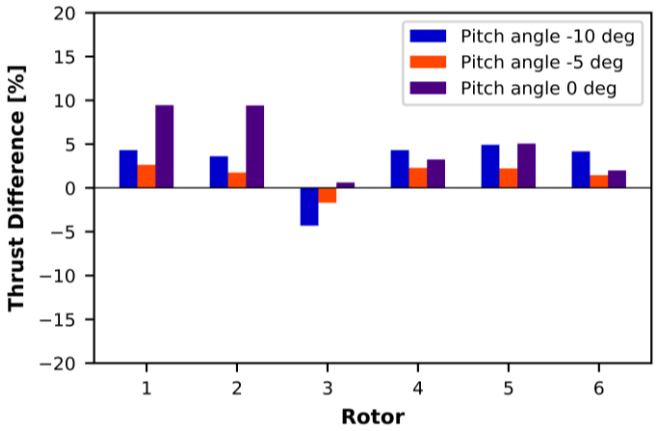

Figure 37: 6-Rotors (Tall) – Discrepancies for 20ft/s TwithB Cases – Thrust.

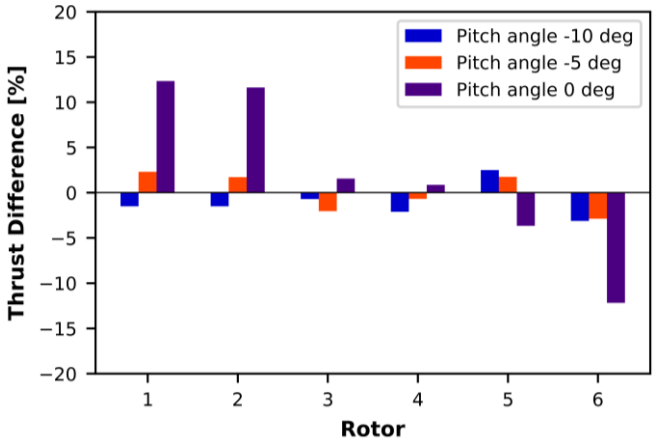

Figure 38: 6-Rotors (Tall) – Discrepancies for 40ft/s TwithB Cases – Thrust.

The discrepancies for the torque values for the TwithB cases also show different trends. For the 20 ft/s wind tunnel speed cases, the discrepancies for torque for the first 4 rotors average about -7% but the discrepancies for the last two rotors is very small across all pitch angles (less than +/- 0.5%), shown in Figure 39. The thrust discrepancies for the 40 ft/s wind tunnel speed cases, were smaller for the middle two rotors (3 and 4) but almost the opposite is observed for the torque discrepancies, see Figure 40. However, the change is much less prominent. The maximum discrepancies for the TwithB cases for thrust and torque are -12.2% and -14.2%, respectively. The average discrepancies for the TwithB cases for thrust and torque were 3.7% and 5.1% respectively.

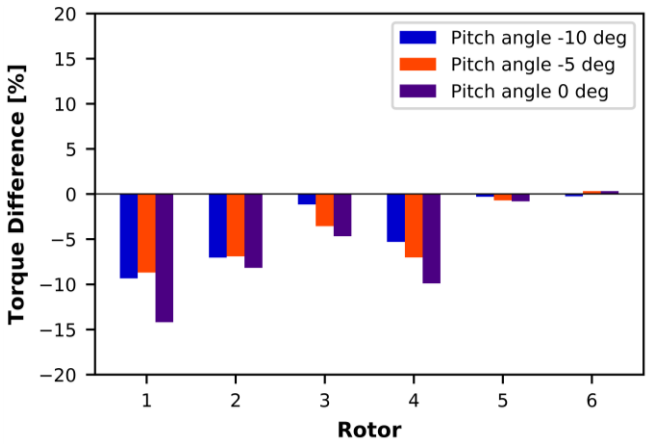

Figure 39: 6-Rotors (Tall) – Discrepancies for 20ft/s TwithB Cases – Torque.

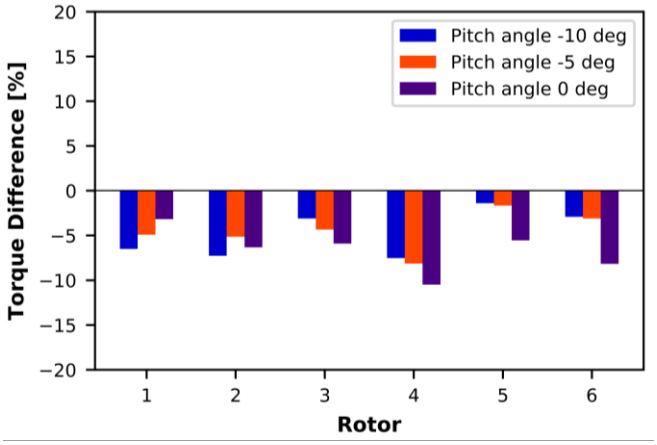

Figure 40: 6-Rotors (Tall) – Discrepancies for 40ft/s TwithB Cases – Torque.

The discrepancies for the FF cases for the tall rotor configuration were actually quite similar to the discrepancies for the TwithB cases. This is very interesting because the rotors in the tall rotor configuration are closer to the ceiling, so it would be expected that the ceiling would have an effect on the flow and that removing the ceiling and walls (as in the FF cases) would cause the simulation to be less accurate. However, the discrepancies for the FF and the TwithB cases are very similar.

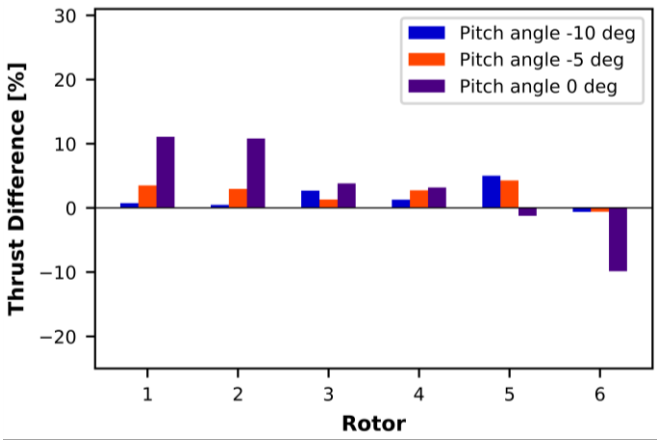

Figure 41: 6-Rotors (Tall) – Discrepancies for 40ft/s FF Cases – Thrust.

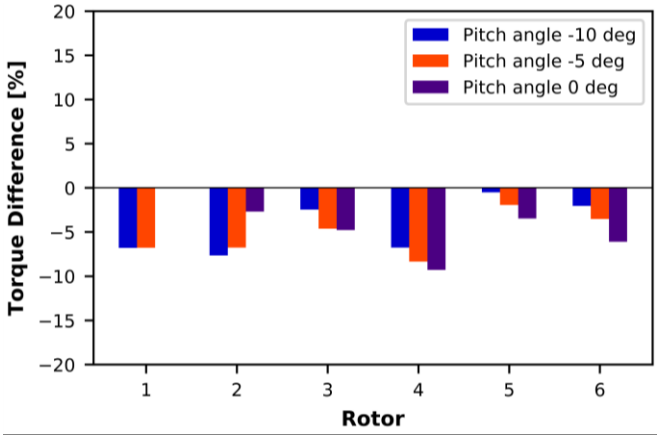

Figure 42: 6-Rotors (Tall) – Discrepancies for 40ft/s FF Cases – Torque.

Figures 43 and 44 show the thrust values for all rotors in the tall rotor configuration for the 20 ft/s and 40 ft/s cases respectively, in order to compare between the RotCFD results and the experimental data for the different rotors at different pitch angles. As discussed there is disagreement between the trends shown in the RotCFD results compared to those shown in the experimental values. The experimental values show thrust is greatest for 0 deg pitch angle whereas the RotCFD values show thrust is greatest for -5 deg pitch angle, followed close by 0 deg pitch angle. The discrepancy between the RotCFD values and the experimental values is much greater for the 0 deg pitch angle case, and very small for the -5 and 0 deg pitch angle cases for the 40 ft/s cases (Figure 44).

Figure 45 shows iso-surfaces drawn at various levels of U-velocity (velocity in the x-direction) to give an impression of the general wake shape for Case 12.3, which was a TwithB case, in the tall rotor configuration, at 20 ft/s tunnel velocity, and at 0 deg pitch angle.

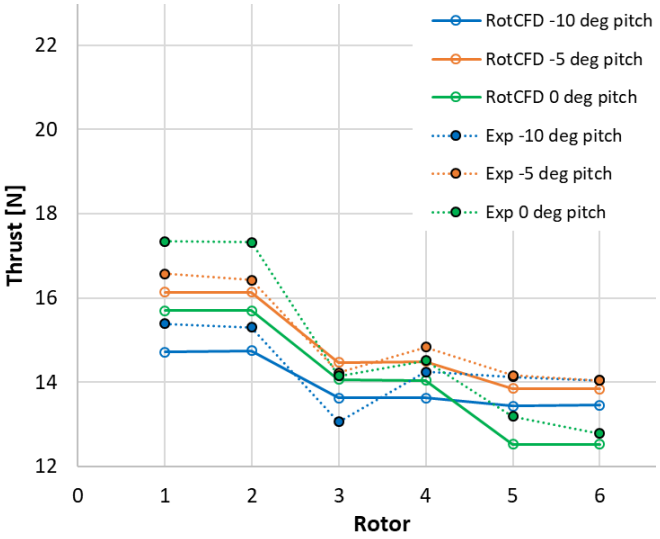

Figure 43: 6-Rotors (Tall) – TwithB vs Experimental Thrust Values for 20 ft/s.

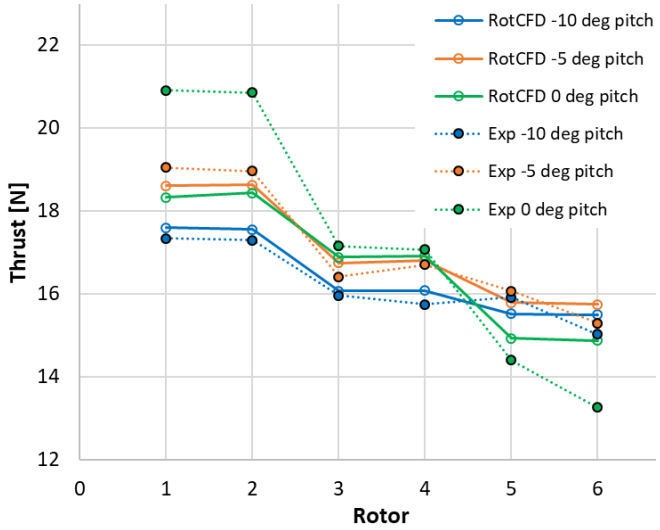

Figure 44: 6-Rotors (Tall) – TwithB vs Experimental Thrust Values for 40 ft/s.

Potential Sources of Error

There are a few sources of potential error from the simulation results and from the experimental data. For the simulation, some of the factors that could have contributed to the uncertainty are the relatively coarse grid, the ADM rotor model, and the airfoil tables. The assumption that all the rotor blades had the exact same geometry, could be another source of error. Only one of the rotor blades was scanned and the airfoil profiles from that blade were used for all of the rotor blades. Blade-to-blade differences will be investigated in future work.

There were some issues in setting up and calibrating the load cells. The load cells will be re-calibrated for the next set of experiments. Additionally, the inclinometer on the MTB was very temperature-sensitive and was recalibrated for each run. A new, more robust inclinometer will be used for future tests. The linear actuators, which tilt the rotors forward and backward did have some backlash, which could also explain why some of the experimental rotor performance data for

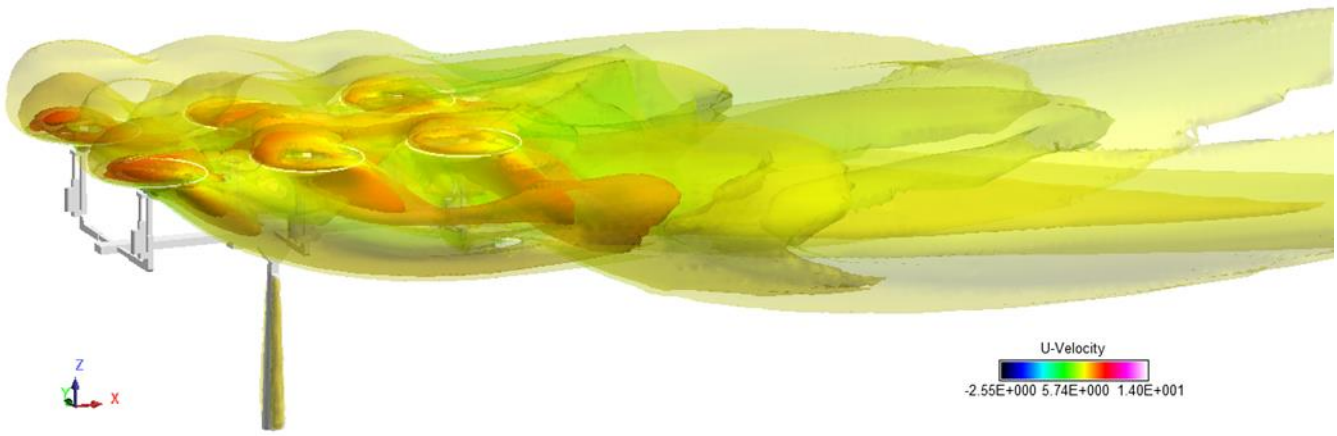

Figure 45: Flow visualization of Case 12.3 – TwithB, Tall Rotor Configuration, 0 deg pitch, 20 ft/s – U-velocity [m/s].

pairs of rotors at the same streamwise location (rotors 1 and 2, 3 and 4, and 5 and 6) did not exhibit equal loads. These actuators will be replaced with more robust linear actuators before the next MTB wind tunnel test. The tunnel data did not include wall corrections or blockage corrections, which could account for some of the discrepancy between the wind tunnel data and the FF cases. Future work may include testing the MTB in a larger wind tunnel facility which would minimize wall effects on the rotor performance and the flowfield. For more details on potential sources of error, see Russell et. al Ref. 4.

CONCLUSION

RotCFD simulations were compared with experimental test data in various rotor configurations. The discrepancies for thrust and torque between the TwithB (in the tunnel with the body) RotCFD results and the experimental test data for the different cases were lowest for the single rotor cases and highest for the four-rotor and six-rotor short cases (see Table 3). This study shows that RotCFD can be used to predict the thrust and torque experimental data values and predict rotor performance trends with changing rotor pitch angle and wind tunnel speed. A summary of the maximum and average discrepancy values for the different TwithB cases is shown in Table 3 and Table 4, respectively. The other rotor performance parameters were not as accurately predicted as the thrust and torque values, but these other values were very small to begin with. For the single rotor cases, the predicted effects that the tunnel had on the flow and the rotor performance were significant, and much larger than the predicted effects that the body had on the flow and rotor performance. The predicted effects of the tunnel on the flow were also prominent when comparing the FF (free field) cases with the TwithB cases for the two-rotor, four-rotor cases, and six-rotor cases in the short rotor configurations. There did not seem to be as large of a difference between the TwithB and the FF cases for the six-rotor cases with the rotors in the tall configuration.

Table 3: Maximum Discrepancy for TwithB Cases

	Max Discrepancy %	
TwithB Cases	Thrust	Torque
Single Rotor	5.6	-7.5
Two-Rotor	5.4	-12.4
Four-Rotor	13.3	-16.6
Six-Rotor Short	-15.7	-14
Six-Rotor Tall	-12.2	-14.2

Table 4: Average Discrepancy for TwithB Cases

	Ave Discrepancy %	
TwithB Cases	Thrust	Torque
Single Rotor	2.7	4.4
Two-Rotor	3.5	7.1
Four-Rotor	8.2	7.5
Six-Rotor Short	5.2	5.3
Six-Rotor Tall	3.7	5.1

FUTURE WORK

The objective in comparing the RotCFD simulation results with the experimental data values was to determine the accuracy of the RotCFD simulations, and how well they correlated with the experimental data values. Having shown that RotCFD simulations can be used to predict the thrust and torque values and trends to a certain degree of accuracy, additional RotCFD simulations can be performed to help determine which configurations should be explored in future MTB tests. Performing wind tunnel tests of the MTB in the U.S. Army 7- by 10-Foot Wind Tunnel is very useful in gathering data on multirotor systems and comparing different configurations. The MTB was designed to have the ability to be tested in many different configurations, however, testing in every single configuration would be impossible within any kind of reasonable test duration. The rotors can be moved forward, backward, up, down, inwards, outwards, and can also tilt forward 90 deg and backwards 5 deg. Additionally, the whole MTB rig can pitch forward 20 deg and backwards 10 deg. RotCFD analysis can be performed on a large number

of cases on the Pleiades supercomputer, much more quickly and for less investment than wind tunnel testing. RotCFD can be run on a workstation as well, but several cases can be completed more quickly on a supercomputer. The results from these simulations can then be used to determine which future testing configurations should be performed in the wind tunnel. Additionally Dorsa Shirazi has been performing simulations of the MTB in a comprehensive analysis code, named Comprehensive Hierarchical Aeromechanics Rotorcraft Model (CHARM). CHARM can model interactional aerodynamics between the rotors, wake, and fuselage of an aircraft. Our aim is to compare the CHARM performance analysis with the RotCFD simulation results. There are also several different CFD software tools available for continued exploration, such as OVERFLOW, with either a rotor actuator disk model or full three-dimensional blade modeling. Knowing the advantages and disadvantages of each, and comparing their results will help each tool to improve and aid in the mission to increase understanding and capability of multirotor systems.

ACKNOWLEDGEMENTS

The authors would like to thank the following people for their contributions to this project. Thank you to William Warmbrodt for his continued outstanding leadership. Thank you to Gloria Yamauchi for her guidance and logistical help in running simulations, and to Dorsa Shirazi for her continued support and contributions to the Aeromechanics CFD Team. Thank you to William Polzin who was an invaluable resource at Sukra Helitek, Inc. Thank you to Larry Meyn who developed the .c81 cleaner script. Additionally thank you to the Aeromechanics Summer Interns that initiated studies of the MTB in RotCFD: Curtis Moffett and Maven Losey.

Gina Willink, lead of the Ames Aeromechanics Mechanical Systems Team, helped throughout the design process, reviewed the design and analysis, and provided invaluable advice. The NASA Machine Shop Team, led by Robert Kornienko and Vincent Derilo, machined the parts of the MTB and provided guidance and helpful suggestions during the design process. Steve Nance along with the other members of the 7- by 10-Foot Wind Tunnel test crew were critical to the project's success.

CONTACT INFORMTATION

All the authors work at NASA Ames Research Center in the Aeromechanics Office. Their emails are listed below.

sarah.a.conley@nasa.gov
carl.r.russell@nasa.gov
kristen.kallstrom@nasa.gov
witold.koning@nasa.gov
ethan.romander@nasa.gov

REFERENCES

[1] C. Russell, G. Willink, Theodore, C, and B. Glasner, "Wind Tunnel and Hover Performance Test Results for Multicopter UAS Vehicles." NASA/TM—2018-219758, February, 2018.

[2] C. Russell and et al, "Multicopter UAS Performance Test 2." NASA/TM—TBD.

[3] G. Cheng, G. Nunez, C. Russell, M. Avera, and J. Dorrerweich, "Wind Tunnel Test Results for an Overlapped Quadrotor Configured UAS," presented at the AHS International 74th Annual Forum and Technology Display, Phoenix, AZ, May 14-17, 2018.

[4] C. Russell and S. Conley, "The Multirotor Test Bed – A New NASA Test Capability for Advanced VTOL Rotorcraft Configurations," submitted to the VFS 76th Annual Forum and Technology Display, Virginia Beach, VA, October 6-8, 2020.

[5] S. Conley and C. Russell, "Mechanical Design of the Multirotor Test Bed," Vertical Flight Society Aeromechanics for Advanced Vertical Flight Technical Meeting, San Jose, CA, January 21-23, 2020.

[6] R. G. Rajagopalan, J. R. Thistle, and W. J. Polzin, "The Potential of GPU Computing for Design in RotCFD," presented at the AHS Technical Meeting on Aeromechanics Design for Transformative Vertical Flight, San Francisco, California, January 16-18, 2018.

[7] R. G. Rajagopalan *et al.*, "RotCFD - A Tool for Aerodynamic Interference of Rotors: Validation and Capabilities," presented at the American Helicopter Society Future Vertical Lift Aircraft Design Conference, January 18-20, 2012, San Francisco, California.

[8] L. A. Novak, K. Guntupalli, and R. G. Rajagopalan, "RotCFD: Advancements in Rotorcraft Modeling and Simulation," presented at the The 4th Asian/Australian Rotorcraft Forum, IISc, India, Nov. 2015.

[9] W. J. F. Koning, "Wind Tunnel Interference Effects on Tiltrotor Testing Using Computational Fluid Dynamics," NASA/CR—2016–219086, March 2016.

[10] W. J. F. A. Koning, "Using RotCFD to Predict Isolated XV-15 Rotor Performance," presented at the AHS Technical Meeting on Aeromechanics Design for Vertical Lift, San Francisco, CA, Jan. 2016, Accessed: Jun. 22, 2020.

[11] M. Losey, "CFD Analysis of a Multirotor Testbed and Airfoils." Aeromechanics Intern Program, Aug. 2019.

[12] M. Drela, "XFOIL: An Analysis and Design System for Low Reynolds Number Airfoils," presented at the Conference on Low Reynolds Number Airfoil Aerodynamics, University of Notre Dame, Jun. 1989.

[13] C. Moffett, "RotCFD Analysis of a Multirotor Test Bed." Aeromechanics Intern Program, Aug. 2018.

[14] W. Johnson, *Rotorcraft Aeromechanics*. Cambridge: Cambridge University Press, 2013.

APPENDIX – Test Matrix

Single Rotor Test Matrix				
Case	**Tunnel Speed [ft/s]**	**MTB Config**	**Pitch [deg]**	**Case Type**
11.1	20	Short	-10	TwithB
11.2	20	Short	-5	TwithB
11.3	20	Short	0	TwithB
11.4	40	Short	-10	TwithB
11.5	40	Short	-5	TwithB
11.6	40	Short	0	TwithB
11.7	20	Short	-10	FF
11.8	20	Short	-5	FF
11.9	20	Short	0	FF
11.1O	40	Short	-10	FF
11.11	40	Short	-5	FF
11.12	40	Short	0	FF
11.13	20	Short	-10	TnoB
11.14	20	Short	-5	TnoB
11.15	20	Short	0	TnoB
11.16	40	Short	-10	TnoB
11.17	40	Short	-5	TnoB
11.18	40	Short	0	TnoB

Two Rotor Test Matrix				
Case	**Tunnel Speed [ft/s]**	**MTB Config**	**Pitch [deg]**	**Case Type**
16.1	20	Short	-10	TwithB
16.2	20	Short	-5	TwithB
16.3	20	Short	0	TwithB
16.4	20	Short	-10	FF
16.5	20	Short	-5	FF
16.6	20	Short	0	FF

Four Rotor Test Matrix				
Case	**Tunnel Speed [ft/s]**	**MTB Config**	**Pitch [deg]**	**Case Type**
15.1	20	Short	-10	TwithB
15.2	20	Short	-5	TwithB
15.3	20	Short	0	TwithB
15.4	20	Short	-10	FF
15.5	20	Short	-5	FF
15.6	20	Short	0	FF

Six Rotor Test Matrix				
Case	**Tunnel Speed [ft/s]**	**MTB Config**	**Pitch [deg]**	**Case Type**
12.1	20	Tall	-10	TwithB
12.2	20	Tall	-5	TwithB
12.3	20	Tall	0	TwithB
12.4	40	Tall	-10	TwithB
12.5	40	Tall	-5	TwithB
12.6	40	Tall	0	TwithB
12.7	20	Tall	-10	FF
12.8	20	Tall	-5	FF
12.9	20	Tall	0	FF
12.1O	40	Tall	-10	FF
12.11	40	Tall	-5	FF
12.12	40	Tall	0	FF
13.1	20	Short	-10	TwithB
13.2	20	Short	-5	TwithB
13.3	20	Short	0	TwithB
13.4	40	Short	-10	TwithB
13.5	40	Short	-5	TwithB
13.6	40	Short	0	TwithB
13.7	20	Short	-10	FF
13.8	20	Short	-5	FF
13.9	20	Short	0	FF
13.1O	40	Short	-10	FF
13.11	40	Short	-5	FF
13.12	40	Short	0	FF